Applied Physics Letters

Thermal transport of monolayer amorphous carbon and boron nitride

Cite as: Appl. Phys. Lett. **120**, 222201 (2022); https://doi.org/10.1063/5.0089967
Submitted: 02 March 2022 • Accepted: 16 May 2022 • Published Online: 31 May 2022

Yu-Tian Zhang (张雨田), Yun-Peng Wang (王云鹏), Yu-Yang Zhang (张余洋), et al.

Applied Physics Letters ARTICLE scitation.org/journal/apl

Thermal transport of monolayer amorphous carbon and boron nitride

Cite as: Appl. Phys. Lett. **120**, 222201 (2022); doi: 10.1063/5.0089967
Submitted: 2 March 2022 · Accepted: 16 May 2022 ·
Published Online: 31 May 2022

Yu-Tian Zhang (张雨田),[1] Yun-Peng Wang (王云鹏),[2,a)] Yu-Yang Zhang (张余洋),[1,a)] Shixuan Du (杜世萱),[1,3] and Sokrates T. Pantelides[1,4,5]

AFFILIATIONS

[1]University of Chinese Academy of Sciences and Institute of Physics, Chinese Academy of Sciences, Beijing 100049, China
[2]Hunan Key Laboratory for Super Microstructure and Ultrafast Process, School of Physics and Electronics, Central South University, Changsha 410083, China
[3]Songshan Lake Materials Laboratory, Dongguan, Guangdong 523808, China
[4]Department of Physics and Astronomy, Vanderbilt University, Nashville, Tennessee 37235, USA
[5]Department of Electrical and Computer Engineering, Vanderbilt University, Nashville, Tennessee 37235, USA

[a)]**Authors to whom correspondence should be addressed:** yunpengwang@csu.edu.cn and zhangyuyang@ucas.ac.cn

ABSTRACT

Amorphous materials feature localization of electrons and phonons that alter the electronic, mechanical, thermal, and magnetic properties. Here, we report calculations of the in-plane thermal conductivities of monolayer amorphous carbon and monolayer amorphous boron nitride, by reverse nonequilibrium molecular dynamics simulations. We find that the thermal conductivities of both monolayer amorphous carbon (MAC) and monolayer amorphous boron nitride (ma-BN) are about two orders of magnitude smaller than their crystalline counterparts. Moreover, the ultralow thermal conductivities are independent of the temperature and strain due to their extremely short heat carrier mean free paths. The relation between the structure disorder and the reduction of the thermal conductivity is analyzed in terms of the vibrational density of states and the participation ratio. The ma-BN shows strong vibrational localization across the frequency range, while the MAC exhibits a unique extended G^* diffuson mode due to its sp^2 hybridization and the broken E_{2g} symmetry. The irregular vibrational patterns are also analyzed. The present results may enable potential applications of MAC and ma-BN in thermal management.

Two-dimensional materials show diverse thermal conducting properties. For example, graphene and monolayer h-BN possess very high thermal conductivity (κ = 2000–5000 Wm^{-1} K^{-1} for graphene[1–4] and ~750 Wm^{-1} K^{-1} for h-BN[5,6]). The high thermal conductivity makes these materials useful in heat-removal applications in nanodevices.[7–12] Meanwhile, some 2D materials, like SnSe, 2D tellurium, selenene, stanene, and MoO_3, exhibit a low κ, which is desirable for thermoelectric devices and thermal protective barriers in nano- and micro-scale devices.[13–16]

There have been several theoretical studies on the thermal conductivity of monolayer amorphous carbon (MAC) and 2D amorphous boron nitride (a-BN) using atomic-structure models obtained by amorphization of crystalline models.[17–20] These amorphization processes produce either a typical Zachariasen continuous random network (Z-CRN)[21] or a defective instead of an amorphous structure. Recent experiments identified monolayer amorphous carbon (MAC) as a CRN structure with embedded nanocrystallites instead of a pure Z-CRN structure in Ref. 22. Recent theoretical work on a-BN reveals the absence of crystallites and the presence of pseudocrystallites, namely, honeycomb structures made of random B–N, B–B, and N–N bonds (noncanonical BN hexagons).[23] Thus, the thermal transport properties of MAC and a-BN are still an open question.

In this work, we study the thermal transport of 2D amorphous carbon and boron nitride with newly established atomic models,[22,23] using reverse nonequilibrium molecular dynamics (RNEMD) simulations. We found that the thermal conductivities of these amorphous materials are significantly lower than those of the corresponding crystalline monolayers and are insensitive to temperature, in contrast to the prominent temperature dependence of their crystalline counterparts. The reduction in thermal conductivity originates from the shorter phonon lifetime and significant localization of vibrational modes. Due to the sp^2-hybridized carbon network and the absence of the E_{2g} symmetry caused by amorphousness, MAC exhibits a unique high-frequency extended G^* mode that resembles the G mode of graphene.

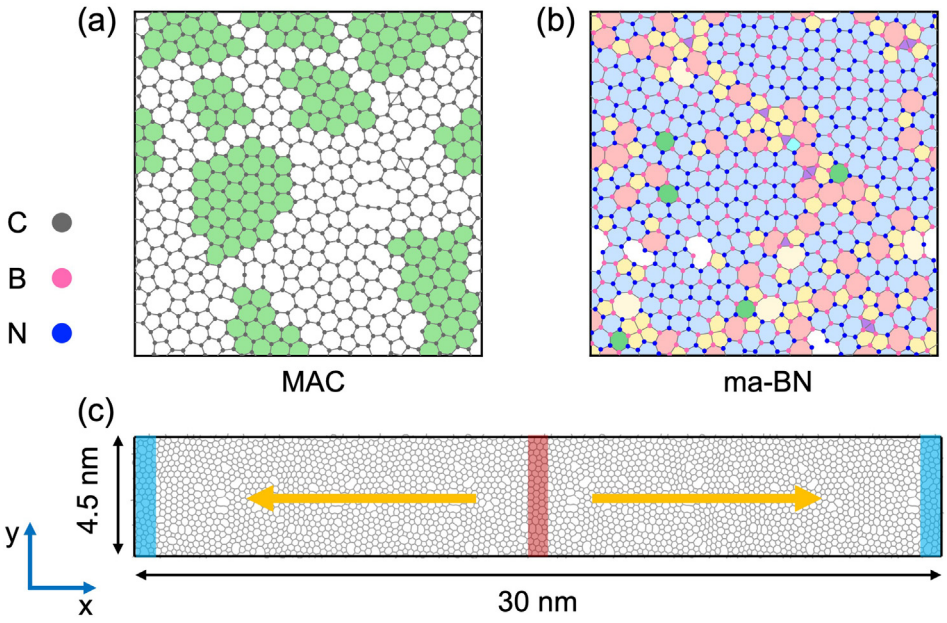

FIG. 1. Atomic structures of MAC and ma-BN. (a) and (b) Typical amorphous structures for MAC and ma-BN, respectively. The sizes of the periodic cells are 45×45 Å^2. The green regions are the crystallites of MAC, and the blue regions are the pseudocrystallites of ma-BN. Pentagon and heptagon are colored in yellow and orange, respectively. (c) A typical supercell of amorphous materials employed in the RNEMD simulation of thermal conductivities. The heat is injected from the middle red bin ("hot" region), and the yellow arrows indicate the heat flow along *x*-directions toward the blue bins in which the heat sinks ("cold" regions).

The atomic structures of MAC and ma-BN are taken from recent works,[22,23] where they were generated by kinetic Monte Carlo (kMC) simulations. Representative equilibrium structures of MAC [CRN with nanocrystallites, as shown in Fig. 1(a)] and ma-BN [CRN with pseudocrystallites, as shown in Fig. 1(b)] are used in subsequent simulations. In the RNEMD simulations, interatomic interactions are described by the optimized Tersoff potential developed by Lindsay and Broido[24] for graphene and MAC, and the extended Tersoff potential (BN-ExTeP[25]) for h-BN and ma-BN. Thermal conductivity was calculated by the RNEMD based on the Muller–Plath algorithm,[26] as implemented in Large-Scale Atomic/Molecular Massively Parallel Simulator (LAMMPS).[27] The periodic supercell for thermal conductivity calculations is depicted in Fig. 1(c) (see Methods in the supplementary material for details).

The thermal conductivities of graphene and h-BN have been studied extensively.[1–6,28–36] We employed the same potential for crystalline and amorphous structures to make the thermal conductivities comparable. The calculated thermal conductivity of crystalline graphene is 2864 Wm^{-1} K^{-1} at 300 K, while the extrapolated phonon mean free path (MFP) for graphene is 516 nm. For monolayer h-BN, the calculated thermal conductivity is 1985 Wm^{-1} K^{-1} at 300 K, and the phonon MFP is 484 nm. The calculated κ of h-BN is larger than both experimental[5,6] and equilibrium MD (EMD) results.[34] We attribute this discrepancy to the different potentials (optimized Tersoff vs BN-ExTeP used in this work). The optimized Tersoff is not used here because ma-BN becomes chain-like and cannot maintain its characteristic pseudocrystallites structures embedded in a pseudo-CRN.[23] For both graphene and h-BN, the thermal conductivities decrease with increasing temperature, as shown in Fig. 2(a). The fitting curves obey power laws of $T^{-1.23}$ for graphene and $T^{-2.28}$ for h-BN. The power-law reduction of κ indicates intensive phonon scattering and shorter phonon MFP at higher temperatures, which is qualitatively consistent with experimental data.[2,3,5,6]

The calculated thermal conductivities of MAC and ma-BN are shown in Fig. 2(b) as functions of temperature. The calculated κ are

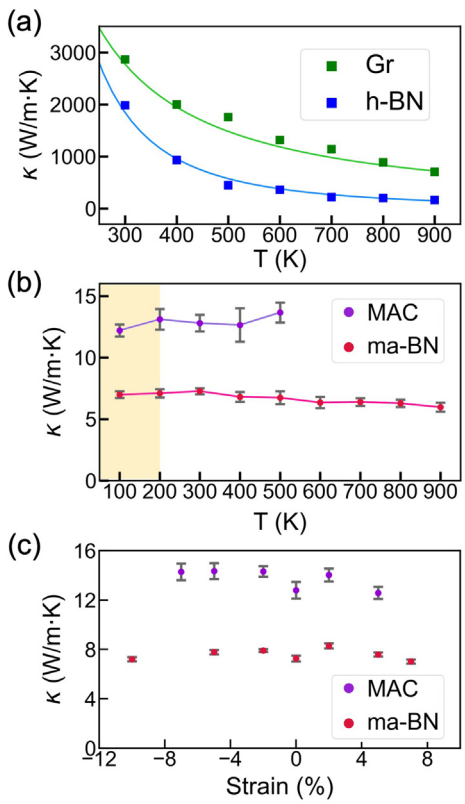

FIG. 2. Thermal conductivities as functions of temperature and strain. (a) Graphene and h-BN. (b) MAC and ma-BN. (MAC is unstable at $T > 500$ K, thus κ values are not shown.) The low-T region in (b) is marked by yellow to indicate the neglect of quantum corrections. (c) 300 K thermal conductivities at different strains. The error bars represent the standard deviations of ten independent calculations.

about 13.3 Wm^{-1} K^{-1} for MAC and 7.2 Wm^{-1} K^{-1} for ma-BN at 300 K. Both of these values are two orders of magnitude lower than their crystalline counterparts. The large reduction of κ is attributed to the amorphous atomic arrangements, which encumber the formation of delocalized phonons and lead to intrinsically short phonon MFP. In the RNEMD framework, no quantum correction at low temperatures is considered,[37] since it is assumed to be negligible for amorphous materials;[17,38] further studies are needed to fully resolve the low-temperature thermal conductivities. The higher κ of MAC compared with that of ma-BN may be due to the longer carrier MFP [see Fig. S1(a)]. These κ values are comparable to some graphene polymorphs like graphdiynes[39] but are higher than the ultralow κ of amorphous macromolecules and Kapitza resistance of amorphous Si/Ge interfaces.[40,41]

Whereas the thermal conductivities of graphene and h-BN drop off as functions of temperature, the κ values of MAC and ma-BN are largely temperature-independent [Fig. 2(b)], except for the slight reduction at $T > 600$ K for ma-BN. The temperature independence of κ for MAC is consistent with the results for strongly defective graphene reported in Ref. 19. On the contrary, MAC in the Z-CRN structure exhibits distinct thermal transport properties, including the value and the temperature dependency of κ.[17] Thus, the thermal conductivity of amorphous 2D materials may serve as an indicator of their atomic structures. The κ values of MAC and ma-BN are also independent of compressive and tensile strains [Fig. 2(c)], distinct from other low-κ materials like silicene and α-Ag_2S.[42,43] The z-direction ripples have negligible influence on the in-plane heat transport (Fig. S3), indicating intrinsically short carrier MFPs and carrier localization lengths.[44–48] We, thus, infer that substrates would have a minor effect on the low thermal conductivities of MAC and ma-BN.

The mechanism of heat transport in amorphous materials is fundamentally different from crystals. Because of the lack of periodicity, the q-vector is no longer a good quantum number in amorphous materials, whereby phonons as the quasiparticle of lattice vibrations are ill-defined;[49] the concept of vibrational density of states (VDOS) is still applicable, though. The widely adopted theory of heat transport in disordered solids was proposed by Allen and Feldman in 1993.[50] They categorized the heat carriers into three types: propagons, diffusons, and locons. Propagons are low-frequency vibrational modes in analogy to the wave-like phonons, while diffusons are of mid-frequency and carry the heat diffusively. Locons are high-frequency vibrational modes and spatially localized; they contribute negligibly to thermal conductivity. As shown below, the low-frequency out-of-plane (ZA) mode, serving as the dominant heat carriers in crystalline graphene and h-BN,[5,31–33] cannot propagate freely in MAC and ma-BN, thus heat cannot be transported effectively and results in the low thermal conductivities. The border between propagons and diffusons is called "Ioffe–Regel crossover," and the boundary between locons and extendons is called "mobility edge"[51] [see Fig. 3(c)].

We calculated the VDOS of MAC and ma-BN, to understand their low and temperature-insensitive thermal conductivities. As shown in Figs. 3(a) and 3(b), the VDOS of both graphene and h-BN shows characteristic peaks, namely, the high-frequency optical modes near 50 THz and the ZA and out-of-plane optical (ZO) mode at ~8 and 16 THz, respectively. The lifetime of heat carriers is inversely proportional to the width of the VDOS peaks,[7,18,52,53] so are their contributions to the thermal conductivity. As for MAC and ma-BN, these characteristic peaks either broaden severely or even disappear, as shown in Figs. 3(a) and 3(b), respectively, indicating a decrease in carrier lifetimes as well as the MFP,[54] therefore resulting in low thermal conductivities. The VDOS alone, however, cannot explain the order-of-magnitude difference in the thermal conductivities of crystalline and amorphous materials because the nonhomogeneity and characteristic feature of amorphous structures are not reflected in the VDOS.

We then analyzed the calculated participation ratio (PR). Defined as the fraction of atoms participating in a particular vibrational mode, the PR measures the localization strength of vibrational modes, fully

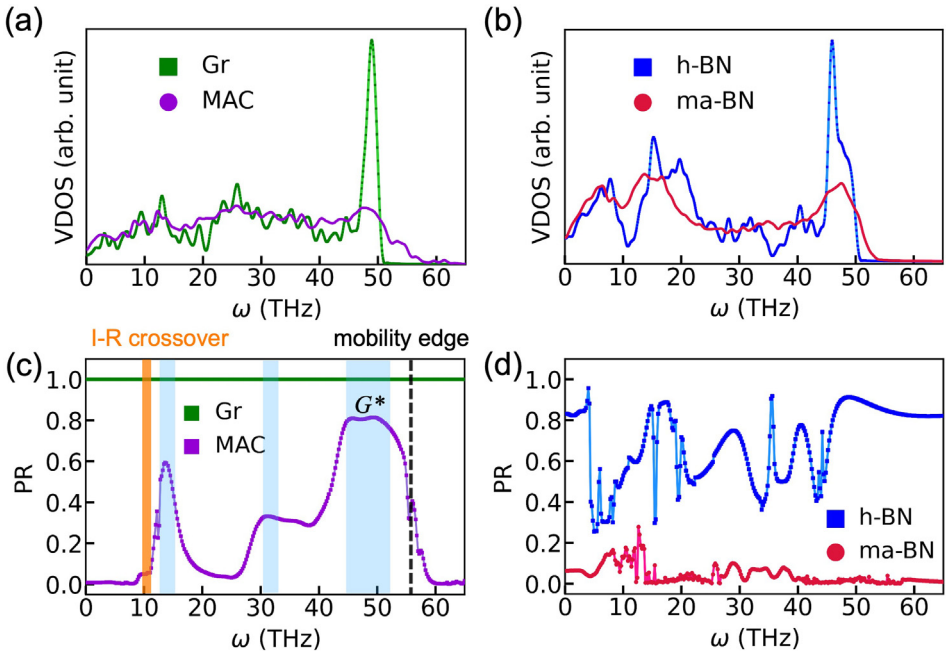

FIG. 3. The vibrational density of states (VDOS) and the participation ratio (PR). (a) and (c) Graphene and MAC. (b) and (d) h-BN and ma-BN. In (c), three extended regions of MAC diffusons are highlighted in light blue, orange line labels the Ioffe–Regel crossover, and black dashed line labels the mobility edge.

reflecting the nonhomogeneity in MAC and ma-BN. The PR of a spatially localized vibrational mode scales inversely with the number of atoms; the PR of a delocalized mode is of order unity.[49] As shown in Fig. 3(c), the calculated PR for graphene is equal to 1 across the frequency range, reflecting the delocalization of all the vibrational modes,[17] rationalizing graphene as the 2D material with the highest thermal conductivity. The calculated PR of h-BN is not uniformly 1 but is always larger than 0.4 in most of the frequency ranges, see Fig. 3(d). Vibrational modes in h-BN are also delocalized, but not as perfectly as in graphene. The inequivalence of boron and nitrogen and the resulting sublattice symmetry breaking may be the reason for the lower PR of h-BN. The low and nonuniform PR for h-BN is the one possible reason for its smaller thermal conductivity than graphene.

The calculated PRs of amorphous materials show prominent reduction compared with their crystalline analogs, revealing the significant localization of vibrational modes in frequency space. It is not surprising to observe strong localization in amorphous materials due to the lack of periodic potential. The disorder-induced localization is not limited to electronic states as originally proposed by Anderson,[44] but is also applicable to spin and vibrational waves in disordered media.[17] The calculated PR for ma-BN is shown in Fig. 3(d); it remains smaller than 0.2 across the whole frequency range, reflecting the additional localization by structural inhomogeneities. Within the high-frequency regime >40 THz, the PR is close to zero; such modes are locons.[50] In the low-frequency regime below 15 THz, the PR is still sizable (0.1–0.2) compared to the corresponding PR of h-BN. Vibrational modes within this regime still propagate, but to a limited extent. These propagons should be the major contributor to the low thermal conductivity of ma-BN. The lower PR of ma-BN may originate from its unique pseudocrystallites, which are structurally more disordered than the crystallites in MAC.

The calculated PR of MAC shows rich features [Fig. 3(c)]. In the low-frequency regime (0–8 THz), the PR is close to zero. There are three regions with large values of PR, as highlighted by blue in Fig. 3(c). These delocalized vibrational modes (PR > 0.4 can be regarded as delocalized[17]) are characteristic of MAC. The prominent PR plateau at 45–55 THz (or 1501–1668 cm^{-1}) corresponds to diffusons, whose frequency range coincides with the well-known G mode of graphene (1580–1600 cm^{-1}). The Raman active G mode originates from an sp^2-bonding.[55] MAC supports the activation of the G mode because it is a sp^2-bonded carbon network. Disorders and impurities can split the G mode into G' (1583 cm^{-1}) and D' modes (1620 cm^{-1}),[56,57] while the small amount of non-sp^2 carbon atoms can broaden the G mode. The amorphousness of MAC merges these modes to form an extended PR plateau as seen in Fig. 3(c). We labeled these extended modes in MAC as the G^* mode to distinguish it from the graphene G mode. The amorphous lattice of MAC breaks the E_{2g} symmetry of graphene; thus, the regular in-plane bond stretching of the G mode is replaced by the irregular out-of-phase vibration of the G^* mode [Fig. 4(c)]. The G^* mode is also supported by prior experimental observations of the broadened D and G modes in MAC.[22,58]

Vibrational modes in amorphous materials are no longer constrained by crystalline symmetry; thus, complex vibrational patterns that are forbidden in a crystal can emerge. The eigenvectors of vibrational modes are another complementary metric for illustrating the localization in real space and can be obtained by solving the secular equation of the dynamical matrix. As shown in Figs. 4(a), 4(b), 4(e), and 4(f), the vibrational patterns of propagons in MAC and ma-BN show a certain degree of periodicity;[49] the atoms vibrate along the same direction within each subregion, i.e., the movements are in-phase. These vibrational modes are not uniform due to the nonhomogeneity imposed by nanocrystallites (MAC) and pseudocrystallites (ma-BN). These highly localized propagons hinder heat transport, explaining the two-orders-of-magnitude reduction of thermal conductivities. Patterns of diffusons lack periodicity, they feature out-of-phase movements with the atoms vibrate along random directions [Figs. 4(c)

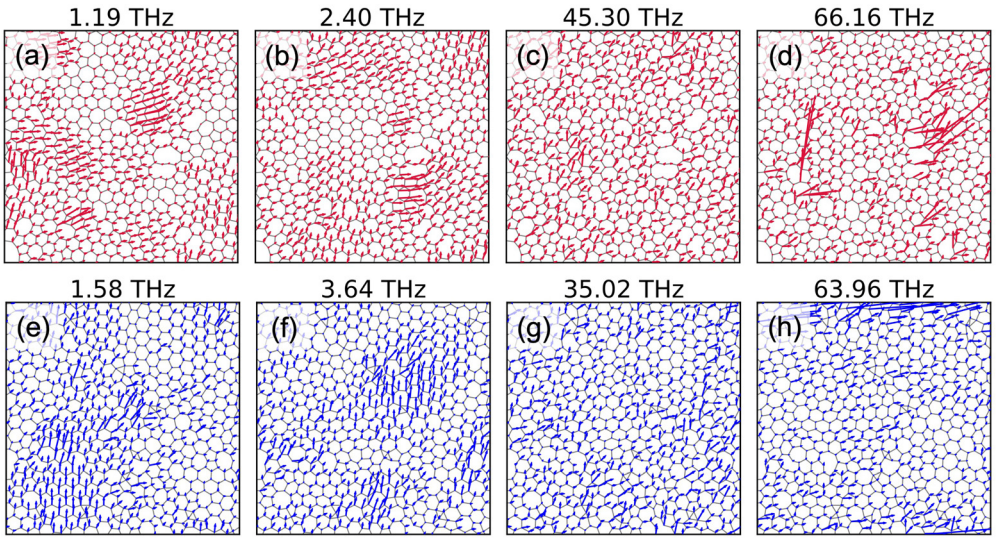

FIG. 4. Vibrational patterns of MAC and ma-BN. Red and blue arrows represent the eigenvectors of each atom. (a)–(d) For MAC and (e)–(h) for ma-BN. (a) and (b) Two low-frequency propagons with collective motions. (c) A mid-frequency diffuson with irregular motion, corresponding to the extended G^* mode. (d) A high-frequency locon mode. (e) and (f) Two low-frequency propagons of ma-BN. (g) A mid-frequency diffuson of ma-BN. (h) A locon of ma-BN.

and 4(g)], while locons are much more spatially confined and also vibrate irregularly [Figs. 4(d) and 4(h)]. These amorphous vibrational patterns are in line with the Allen–Feldman picture.[50,51]

In summary, we present a comprehensive investigation of the vibrational and thermal transport properties of MAC and ma-BN. We find that the thermal conductivities of MAC and ma-BN are temperature-/strain-independent and are about two orders of magnitude smaller than their crystalline counterparts at room temperature. Our analysis of the VDOS shows that the reduction of the thermal conductivity can be explained by the short lifetime of heat carriers in amorphous structures. Moreover, the amorphous vibrational modes exhibit localization evidenced by the reduction in the PR. Different from the strong localization of ma-BN across the frequency range, MAC exhibits three extended diffuson modes. The characteristic G^* mode originates from the sp^2 carbon network and the broken E_{2g} symmetry. Graphene and h-BN show high thermal conductivities, which is desirable in heat dissipation applications; for their amorphous counterparts, we show that MAC and ma-BN possess intrinsic low thermal conductivities that do not vary with temperature and strain, thus, desirable in thermal-isolation applications. The intrinsic low thermal conductivities of MAC and ma-BN should also be immune to the interface of hybrid lateral heterostructures, as shown in other works.[19] In addition to the electrical insulating properties and good stability at room temperature,[22,23] MAC and ma-BN are promising candidates for thermal management applications.

See the supplementary material for the details of methods of thermal conductivity calculations and additional data.

We acknowledge financial support from the National Key R&D Program of China (Nos. 2019YFA0308500 and 2018YFA0305800), the National Natural Science Foundation of China (Nos. 61888102, 12004439, and 51922011), the Strategic Priority Research Program of the Chinese Academy of Sciences (Nos. XDB30000000 and XDB28000000), the K. C. Wong Education Foundation, and the Fundamental Research Funds for the Central Universities. Work at Vanderbilt was funded by the McMinn Endowment.

AUTHOR DECLARATIONS

Conflict of Interest

The authors have no conflicts to disclose.

DATA AVAILABILITY

The data that support the findings of this study are available from the corresponding authors upon reasonable request.

REFERENCES

[1]A. A. Balandin, S. Ghosh, W. Bao, I. Calizo, D. Teweldebrhan, F. Miao, and C. N. Lau, "Superior thermal conductivity of single-layer graphene," Nano Lett. **8**, 902 (2008).
[2]J.-U. Lee, D. Yoon, H. Kim, S. W. Lee, and H. Cheong, "Thermal conductivity of suspended pristine graphene measured by Raman spectroscopy," Phys. Rev. B **83**, 081419(R) (2011).
[3]S. Chen, Q. Wu, C. Mishra, J. Kang, H. Zhang, K. Cho, W. Cai, A. A. Balandin, and R. S. Ruoff, "Thermal conductivity of isotopically modified graphene," Nat. Mater. **11**, 203 (2012).
[4]X. Xu, L. F. Pereira, Y. Wang, J. Wu, K. Zhang, X. Zhao, S. Bae, C. Tinh Bui, R. Xie, J. T. Thong, B. H. Hong, K. P. Loh, D. Donadio, B. Li, and B. Ozyilmaz, "Length-dependent thermal conductivity in suspended single-layer graphene," Nat. Commun. **5**, 3689 (2014).
[5]Q. Cai, D. Scullion, W. Gan, A. Falin, S. Zhang, K. Watanabe, T. Taniguchi, Y. Chen, E. J. G. Santos, and L. H. Li, "High thermal conductivity of high-quality monolayer boron nitride and its thermal expansion," Sci. Adv. **5**, eaav0129 (2019).
[6]Q. Cai, D. Scullion, W. Gan, A. Falin, P. Cizek, S. Liu, J. H. Edgar, R. Liu, B. C. C. Cowie, E. J. G. Santos, and L. H. Li, "Outstanding thermal conductivity of single atomic layer isotope-modified boron nitride," Phys. Rev. Lett. **125**, 085902 (2020).
[7]A. A. Balandin, "Thermal properties of graphene and nanostructured carbon materials," Nat. Mater. **10**, 569 (2011).
[8]E. Pop, V. Varshney, and A. K. Roy, "Thermal properties of graphene: Fundamentals and applications," MRS Bull. **37**, 1273 (2012).
[9]Z. Yan, G. Liu, J. M. Khan, and A. A. Balandin, "Graphene quilts for thermal management of high-power GaN transistors," Nat. Commun. **3**, 827 (2012).
[10]A. L. Moore and L. Shi, "Emerging challenges and materials for thermal management of electronics," Mater. Today **17**, 163 (2014).
[11]H. Han, Y. Zhang, N. Wang, M. K. Samani, Y. Ni, Z. Y. Mijbil, M. Edwards, S. Xiong, K. Saaskilahti, M. Murugesan, Y. Fu, L. Ye, H. Sadeghi, S. Bailey, Y. A. Kosevich, C. J. Lambert, J. Liu, and S. Volz, "Functionalization mediates heat transport in graphene nanoflakes," Nat. Commun. **7**, 11281 (2016).
[12]D. L. Nika and A. A. Balandin, "Phonons and thermal transport in graphene and graphene-based materials," Rep. Prog. Phys. **80**, 036502 (2017).
[13]B. Peng, H. Zhang, H. Shao, Y. Xu, X. Zhang, and H. Zhu, "Low lattice thermal conductivity of stanene," Sci. Rep. **6**, 20225 (2016).
[14]Z. Gao, F. Tao, and J. Ren, "Unusually low thermal conductivity of atomically thin 2D tellurium," Nanoscale **10**, 12997 (2018).
[15]G. Liu, Z. Gao, G.-L. Li, and H. Wang, "Abnormally low thermal conductivity of 2D selenene: An *ab initio* study," J. Appl. Phys. **127**, 065103 (2020).
[16]Z. Tong, T. Dumitrica, and T. Frauenheim, "Ultralow thermal conductivity in two-dimensional MoO_3," Nano Lett. **21**, 4351 (2021).
[17]T. Zhu and E. Ertekin, "Phonons, localization, and thermal conductivity of diamond nanothreads and amorphous graphene," Nano Lett. **16**, 4763 (2016).
[18]B. Mortazavi, Z. Fan, L. F. C. Pereira, A. Harju, and T. Rabczuk, "Amorphized graphene: A stiff material with low thermal conductivity," Carbon **103**, 318 (2016).
[19]S. Bazrafshan and A. Rajabpour, "Thermal transport engineering in amorphous graphene: Non-equilibrium molecular dynamics study," Int. J. Heat Mass Transfer **112**, 379 (2017).
[20]X. Wu and Q. Han, "Thermal conductivity of monolayer hexagonal boron nitride: From defective to amorphous," Comput. Mater. Sci. **184**, 109938 (2020).
[21]W. H. Zachariasen, "The atomic arrangement in glass," J. Am. Chem. Soc. **54**, 3841 (1932).
[22]C. T. Toh, H. Zhang, J. Lin, A. S. Mayorov, Y. P. Wang, C. M. Orofeo, D. B. Ferry, H. Andersen, N. Kakenov, Z. Guo, I. H. Abidi, H. Sims, K. Suenaga, S. T. Pantelides, and B. Ozyilmaz, "Synthesis and properties of free-standing monolayer amorphous carbon," Nature **577**, 199 (2020).
[23]Y.-T. Zhang, Y.-P. Wang, X. Zhang, Y.-Y. Zhang, S. Du, and S. T. Pantelides, "The structure of amorphous two-dimensional materials: Elemental monolayer amorphous carbon versus binary monolayer amorphous boron nitride," arXiv:2106.10489 (2021).
[24]L. Lindsay and D. A. Broido, "Optimized Tersoff and Brenner empirical potential parameters for lattice dynamics and phonon thermal transport in carbon nanotubes and graphene," Phys. Rev. B **81**, 205441 (2010).
[25]J. H. Los, J. M. H. Kroes, K. Albe, R. M. Gordillo, M. I. Katsnelson, and A. Fasolino, "Extended Tersoff potential for boron nitride: Energetics and elastic properties of pristine and defective *h*-BN," Phys. Rev. B **96**, 184108 (2017).
[26]F. Muller-Plathe, "A simple nonequilibrium molecular dynamics method for calculating the thermal conductivity," J. Chem. Phys. **106**, 6082 (1997).
[27]S. Plimpton, "Fast parallel algorithms for short-range molecular dynamics," J. Comput. Phys. **117**, 1–19 (1995).
[28]M. Park, S.-C. Lee, and Y.-S. Kim, "Length-dependent lattice thermal conductivity of graphene and its macroscopic limit," J. Appl. Phys. **114**, 053506 (2013).

[29]Z. Wei, J. Yang, K. Bi, and Y. Chen, "Mode dependent lattice thermal conductivity of single layer graphene," J. Appl. Phys. **116**, 153503 (2014).
[30]B. D. Kong, S. Paul, M. B. Nardelli, and K. W. Kim, "First-principles analysis of lattice thermal conductivity in monolayer and bilayer graphene," Phys. Rev. B **80**, 033406 (2009).
[31]L. Lindsay, D. A. Broido, and N. Mingo, "Flexural phonons and thermal transport in graphene," Phys. Rev. B **82**, 115427 (2010).
[32]L. Lindsay, W. Li, J. Carrete, N. Mingo, D. A. Broido, and T. L. Reinecke, "Phonon thermal transport in strained and unstrained graphene from first principles," Phys. Rev. B **89**, 155426 (2014).
[33]T. Feng and X. Ruan, "Four-phonon scattering reduces intrinsic thermal conductivity of graphene and the contributions from flexural phonons," Phys. Rev. B **97**, 045202 (2018).
[34]A. I. Khan, I. A. Navid, M. Noshin, and S. Subrina, "Thermal transport characterization of hexagonal boron nitride nanoribbons using molecular dynamics simulation," AIP Adv. **7**, 105110 (2017).
[35]R. D'Souza and S. Mukherjee, "Length-dependent lattice thermal conductivity of single-layer and multilayer hexagonal boron nitride: A first-principles study using the Callaway–Klemens and real-space supercell methods," Phys. Rev. B **96**, 205422 (2017).
[36]L. Lindsay and D. A. Broido, "Enhanced thermal conductivity and isotope effect in single-layer hexagonal boron nitride," Phys. Rev. B **84**, 155421 (2011).
[37]M. Khalkhali and F. Khoeini, "Impact of torsion and disorder on the thermal conductivity of Si nanowires: A nonequilibrium molecular dynamics study," J. Phys. Chem. Solids **112**, 216 (2018).
[38]A. Antidormi, L. Colombo, and S. Roche, "Thermal transport in amorphous graphene with varying structural quality," 2D Mater. **8**, 015028 (2020).
[39]S. M. Hatam-Lee, A. Rajabpour, and S. Volz, "Thermal conductivity of graphene polymorphs and compounds: From C3N to graphdiyne lattices," Carbon **161**, 816 (2020).
[40]A. Giri, P. E. Hopkins, J. G. Wessel, and J. C. Duda, "Kapitza resistance and the thermal conductivity of amorphous superlattices," J. Appl. Phys. **118**, 165303 (2015).
[41]X. Xie, K. Yang, D. Li, T.-H. Tsai, J. Shin, P. V. Braun, and D. G. Cahill, "High and low thermal conductivity of amorphous macromolecules," Phys. Rev. B **95**, 035406 (2017).
[42]W.-X. Zhou, D. Wu, G. Xie, K.-Q. Chen, and G. Zhang, "α-Ag2S: A ductile thermoelectric material with high *ZT*," ACS Omega **5**, 5796 (2020).
[43]B. Ding, X. Li, W. Zhou, G. Zhang, and H. Gao, "Anomalous strain effect on the thermal conductivity of low-buckled two-dimensional silicene," Natl. Sci. Rev. **8**, nwaa220 (2021).
[44]P. W. Anderson, "Absence of diffusion in certain random lattices," Phys. Rev. **109**, 1492 (1958).
[45]P. A. Lee and T. V. Ramakrishnan, "Disordered electronic systems," Rev. Mod. Phys. **57**, 287 (1985).
[46]I. Savić, N. Mingo, and D. A. Stewart, "Phonon transport in isotope-disordered carbon and boron-nitride nanotubes: Is localization observable?," Phys. Rev. Lett. **101**, 165502 (2008).
[47]M. N. Luckyanova, J. Mendoza, H. Lu, B. Song, S. Huang, J. Zhou, M. Li, Y. Dong, H. Zhou, and J. Garlow, "Phonon localization in heat conduction," Sci. Adv. **4**, eaat9460 (2018).
[48]T. Juntunen, O. Vänskä, and I. Tittonen, "Anderson localization quenches thermal transport in aperiodic superlattices," Phys. Rev. Lett. **122**, 105901 (2019).
[49]W. X. Zhou, Y. Cheng, K. Q. Chen, G. Xie, T. Wang, and G. Zhang, "Thermal conductivity of amorphous materials," Adv. Funct. Mater. **30**, 1903829 (2020).
[50]P. B. Allen and J. L. Feldman, "Thermal conductivity of disordered harmonic solids," Phys. Rev. B **48**, 12581 (1993).
[51]P. B. Allen, J. L. Feldman, J. Fabian, and F. Wooten, "Diffusons, locons and propagons: Character of atomie yibrations in amorphous Si," Philos. Mag. B **79**, 1715 (1999).
[52]A. J. Ladd, B. Moran, and W. G. Hoover, "Lattice thermal conductivity: A comparison of molecular dynamics and anharmonic lattice dynamics," Phys. Rev. B **34**, 5058 (1986).
[53]J. E. Turney, E. S. Landry, A. J. H. McGaughey, and C. H. Amon, "Predicting phonon properties and thermal conductivity from anharmonic lattice dynamics calculations and molecular dynamics simulations," Phys. Rev. B **79**, 064301 (2009).
[54]M. Zhou, T. Liang, B. Wu, J. Liu, and P. Zhang, "Phonon transport in antisite-substituted hexagonal boron nitride nanosheets: A molecular dynamics study," J. Appl. Phys. **128**, 234304 (2020).
[55]A. C. Ferrari and J. Robertson, "Interpretation of Raman spectra of disordered and amorphous carbon," Phys. Rev. B **61**, 14095 (2000).
[56]X. Dong, Y. Shi, Y. Zhao, D. Chen, J. Ye, Y. Yao, F. Gao, Z. Ni, T. Yu, and Z. Shen, "Symmetry breaking of graphene monolayers by molecular decoration," Phys. Rev. Lett. **102**, 135501 (2009).
[57]C. Cong and T. Yu, "Evolution of Raman G and G′(2D) modes in folded graphene layers," Phys. Rev. B **89**, 235430 (2014).
[58]W. J. Joo, J. H. Lee, Y. Jang, S. G. Kang, Y. N. Kwon, J. Chung, S. Lee, C. Kim, T. H. Kim, C. W. Yang, U. J. Kim, B. L. Choi, D. Whang, and S. W. Hwang, "Realization of continuous Zachariasen carbon monolayer," Sci. Adv. **3**, e1601821 (2017).